Atmospheric
Chemistry
and Physics

Taehwa Research Forest: a receptor site for severe domestic pollution events in Korea during 2016

John T. Sullivan[1], Thomas J. McGee[1], Ryan M. Stauffer[1,2], Anne M. Thompson[1], Andrew Weinheimer[3], Christoph Knote[4], Scott Janz[1], Armin Wisthaler[5,6], Russell Long[7], James Szykman[7,8], Jinsoo Park[9], Youngjae Lee[9], Saewung Kim[10], Daun Jeong[10], Dianne Sanchez[10], Laurence Twigg[1,11], Grant Sumnicht[1,11], Travis Knepp[8,12], and Jason R. Schroeder[13]

[1]Atmospheric Chemistry and Dynamics Laboratory, NASA Goddard Space Flight Center, Greenbelt, MD 20771, USA
[2]Universities Space Research Association, Columbia, MD 21046, USA
[3]National Center for Atmospheric Research, Boulder, CO 80305, USA
[4]Meteorologisches Institut, Ludwig-Maximilians-Universität München, München, Germany
[5]Department of Chemistry, University of Oslo, Oslo, Norway
[6]Institute for Ion Physics and Applied Physics, University of Innsbruck, Innsbruck, Austria
[7]US EPA/Office of Research and Development/National Exposure Research Lab, Research Triangle Park, NC 27711, USA
[8]NASA Langley Research Center, Hampton, VA 2368, USA
[9]National Institute of Environmental Research, Incheon, South Korea
[10]Department of Earth System Science, University of California, Irvine, Irvine, CA, USA
[11]Science Systems and Applications, Inc., Lanham, MD 20706, USA
[12]Science Systems and Applications, Inc., Hampton, VA 23666, USA
[13]California Air Resources Board, Sacramento, CA 95814, USA

Correspondence: John T. Sullivan (john.t.sullivan@nasa.gov)

Abstract. During the May–June 2016 International Cooperative Air Quality Field Study in Korea (KORUS-AQ), light synoptic meteorological forcing facilitated Seoul metropolitan pollution outflow to reach the remote Taehwa Research Forest (TRF) site and cause regulatory exceedances of ozone on 24 days. Two of these severe pollution events are thoroughly examined. The first, occurring on 17 May 2016, tracks transboundary pollution transport exiting eastern China and the Yellow Sea, traversing the Seoul Metropolitan Area (SMA), and then reaching TRF in the afternoon hours with severely polluted conditions. This case study indicates that although outflow from China and the Yellow Sea were elevated with respect to chemically unperturbed conditions, the regulatory exceedance at TRF was directly linked in time, space, and altitude to urban Seoul emissions. The second case studied, which occurred on 9 June 2016, reveals that increased levels of biogenic emissions, in combination with amplified urban emissions, were associated with severe levels of pollution and a regulatory exceedance at TRF. In summary, domestic emissions may be causing more pollution than by transboundary pathways, which have been historically believed to be the major source of air pollution in South Korea. The case studies are assessed with multiple aircraft, model (photochemical and meteorological) simulations, in situ chemical sampling, and extensive ground-based profiling at TRF. These observations clearly identify TRF and the surrounding rural communities as receptor sites for severe pollution events associated with Seoul outflow, which will result in long-term negative effects to both human health and agriculture in the affected areas.

1 Introduction

The spatiotemporal characteristics of ozone (O_3), nitrogen dioxide (NO_2) and other urban pollutants have been monitored at the ground level within the Seoul Metropolitan Area (SMA) and throughout the Republic of Korea (commonly referred to as South Korea) for several decades (Seo et al., 2014). Although transboundary transport events from other countries (e.g., China) have been demonstrated (Choi et al., 2014), several studies have clearly illustrated the impacts of domestic pollutants on rural receptor sites downwind of the SMA (Kim et al., 2007; Jeon et al., 2014). Furthermore, negative effects associated with poor air quality in South Korea (Ghim et al., 2005) have been connected with increased mortality rates (Lee et al., 2000), and reduction in agricultural yields (Wang and Mauzerall, 2004).

Recent work with high-resolution satellite records from Duncan et al. (2016) indicate a decreasing trend in tropospheric NO_2 columns throughout the SMA from 2005 to 2014 that has been attributed to regulatory (e.g., vehicular) controls or a transition to low- or zero-emissions vehicles (Wang et al., 2014). However, during this same time period, the observed trend has increased near the petrochemical and industrial regions to the west and southwest of the SMA. Therefore, due to the complexities and heterogeneity of emissions within the SMA (Vellingiri et al., 2015), it is important to assess chemical gradients that may occur among sites with varying distances from emission sources (Ryu et al., 2013; Iqbal et al., 2014; Jeon et al., 2014; Lee et al., 2014), including sites that may be rural pollution receptor sites.

While a dense network of ground level observations over South Korea exists to monitor pollution, information regarding O_3 and its precursors (e.g., oxides of nitrogen; volatile organic compounds or VOCs, including biogenic VOCs or BVOCs) above the surface has been sparse. Because of the lack of chemical profiles, it is difficult to characterize O_3 and other pollutants in the air and quantify the impacts of vertical mixing down to the ground level. Analyses of vertical profiles of O_3 at the Olympic Park (OLY, 37.5232° N, 127.1260° E, 26 m a.s.l.) site within the SMA indicate photochemical O_3 production in the afternoon hours corresponding mainly to local precursor advection from upwind regions (the western part of SMA). More recent findings describe the highest O_3 events occurring at rural sites 30 km (Taehwa Forest: TRF, 37.3123° N, 127.3106° E, 160 m a.s.l.; Kim et al., 2013) and 100 km (Chuncheon, 37.881° N, 127.676° E; Jeon et al., 2014) from the SMA. Both of those studies linked the high-pollution events to mobile (vehicular) source emissions in the presence of natural biogenic emissions (i.e., advection of SMA emissions away from their origins and into a high-BVOC environment of increased O_3 production efficiency).

To further investigate the vertical distribution of pollutants impacting South Korea, the United States (US) National Aeronautics and Space Administration (NASA) and the Korean Ministry of the Environment/Korean National Institute of Environmental Research (NIER) conducted an international cooperative field experiment with sampling at both the TRF and OLY sites, entitled the Korea–US Air Quality (KORUS-AQ, https://espo.nasa.gov/home/korus-aq/content/KORUS-AQ, last access: 27 March 2019) study. The KORUS-AQ observation period was specifically chosen to target local photochemical pollution (which peaks in May–June) rather than pollution transport which tends to be greatest in March–April. Differences in daily average (24 h) NO_x ($NO + NO_2$, Fig. 1c) and maximum daily hourly O_3 (Fig. 1d) during the KORUS-AQ study are presented from 10 May to 11 June 2016. NO_x (which is predominantly NO_2 during daytime) can rapidly form O_3 in the presence of VOCs and favorable meteorology. The two largest sources within the South Korea NO_x emissions inventory are (1) mobile or vehicular (such as trucks, passenger cars, taxis, motorcycles, totaling 41.7 %) and (2) "other" mobile sources (such as construction or agricultural machinery, trains, aircraft, ships, totaling 20.0 %) (Lee et al., 2011).

The prevalence of vehicular emissions is apparent in the urban environment (Fig. 1c) with NO_x amounts at OLY frequently an order of magnitude greater than those at rural TRF. Herman et al. (2018) has further shown during the KORUS-AQ study that the difference between TRF (also referred to as Taehwa Mountain) and OLY in columnar NO_2 can be as much as 3.0 DU (Dobson units, $1 \, DU = 2.69 \times 10^{16}$ molecules cm^{-2}). The concentrations of surface O_3 at TRF during stagnant flow regimes far exceeded those at OLY (Fig. 1d) on several days during the study, indicating O_3 formation within the SMA is VOC limited, due to the overabundance of NO_x (Jeon et al., 2012, 2014). However, O_3 formation can rapidly increase as the distance from NO_x sources increases. Recent chemical simulations performed during the KORUS-AQ period by Miyazaki et al. (2018) also reveal that observed boundary layer O_3 can be as much as a 30 ppbv (parts per billion by volume) difference between dynamic and stagnant flow regimes. Supporting work at TRF has also shown that fast oxidation rates (Kim, 2018) and overall oxidation capacity (Jeong et al., 2018) at TRF can exacerbate severe pollution events.

The differences in daily maximum hourly O_3 between the TRF and OLY sites vary from day to day, but the sites had mean and 1 h maximum concentrations of 86.1 ± 21.9 and 80.4 ± 17.5 ppbv, respectively. The South Korean national standard for O_3 is 100 ppbv for a 1 h average and 60 ppbv for an 8 h average (http://eng.me.go.kr/eng/web/index.do?menuId=253, last access: 27 March 2019). Both sites exceeded the 8 h standard 24 times between 10 May and 10 June 2016. However, TRF exceeded the national 1 h standard 11 times, whereas OLY exceeded on only 3 days. These daily and diurnally varying O_3 amounts during the KORUS-AQ study at TRF are described with back-trajectories (Sect. 2.1), synoptic meteorology (Sect. 2.2), and balloon-borne profiles from TRF (Sect. 3.1.1). Since the evo-
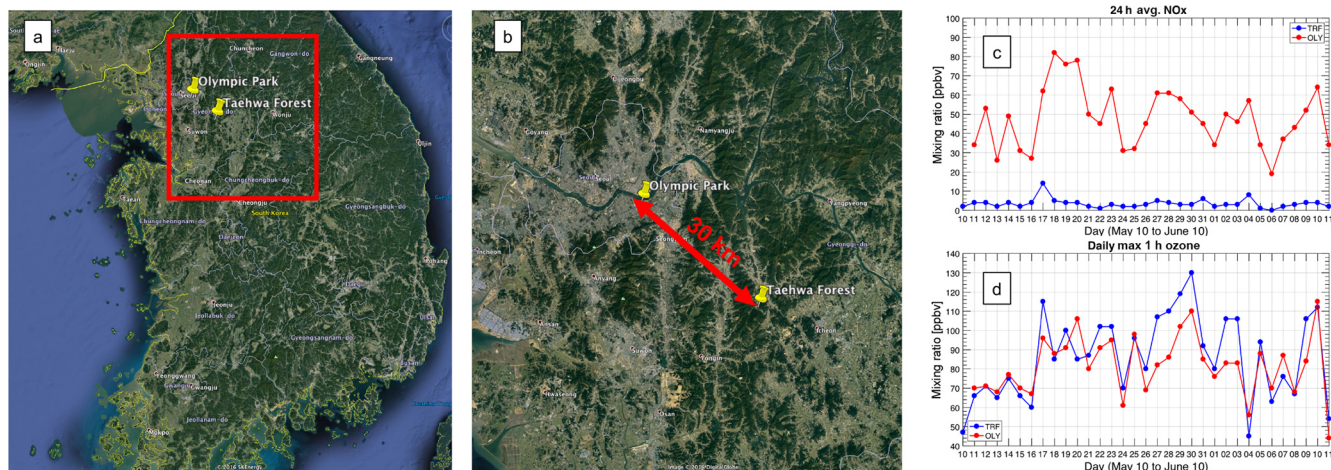
Figure 1. (a) Map of the Korean Peninsula, **(b)** inset view (red square from **a**) of the Olympic Park and Taehwa Research Forest sites, **(c)** daily average NO$_x$ and **(d)** maximum hourly O$_3$ at the TRF and OLY sites.

lution of plume composition is a critical component in understanding severe O$_3$ exceedances, two contrasting case studies (17 May, Sect. 3.2, and 9 June, Sect. 3.3) of the 11 TRF 1 h exceedances are examined with aircraft and ground-based measurements including O$_3$ lidar and ceilometer backscatter profiles. These are complemented by a photochemical box model used to calculate net O$_3$ production and are used distinguish urban and industrial emissions from one of mixed urban and biogenic origins (Sect. 4).

2 Meteorological analyses

2.1 Back-trajectories

To understand variations in the air mass history as it is advected towards TRF, 4-D (time, height, latitude, longitude) back-trajectories were simulated for every day during the KORUS-AQ study (Fig. 2). The back-trajectory calculations were performed using the Lagrangian FLEXible PARTicle dispersion model (FLEXPART, http://flexpart.eu, last access: 27 March 2019; Brioude et al., 2013), driven by the WRF (Weather Research and Forecasting) model meteorology at 3 km spatial resolution. For this simulation, thousands of "air parcels" were released at 15:00 KST (Korean Standard Time; UTC +9 h), and their spatial and vertical (Fig. 2b) trajectory locations were followed back in time for 6 h. Chaotic processes like turbulence or convection were applied in a stochastic manner to each parcel. At hourly intervals the concentration of parcels in each cell of a regular grid was calculated, thus providing the best statistical estimate of the air mass location and altitude prior to reaching TRF.

Red trajectory paths in Fig. 2 are used to identify air masses that were associated with the 11 O$_3$ exceedance days at TRF (based on the South Korean national standard of 1 h standard of 100 ppbv in Fig. 1d). Two of these days,

17 May and 9 June (detailed in Sect. 4), are shown in yellow and orange, respectively. Conversely, days where the daily 1 h O$_3$ at TRF did not exceed 100 ppbv are shown in blue. Days that exceeded the 1 h standard had generally shorter trajectory paths, indicating they were associated with more stagnant conditions and weaker synoptic forcing. The altitudes of exceedance day air masses (Fig. 2b) were also much closer to the surface (thus closer to ground level anthropogenic and biogenic emissions) as compared to non-exceedance days. Exceedance days at TRF were also associated with air masses that flowed through or near the southern portion of the SMA, where they were more likely to interact with local anthropogenic and industrial emission sources (Iqbal et al., 2014).

2.2 Geopotential height anomalies

The Modern-Era Retrospective analysis for Research and Applications Version 2 (MERRA-2, https://gmao.gsfc.nasa.gov/reanalysis/MERRA-2/, last access: 27 March 2019; Gelaro et al., 2017) 500 hPa geopotential heights and anomalies (1981–2010 base period) are presented for 17 May (Fig. 3a) and 9 June 2016 (Fig. 3b) at 21:00 KST. An upper-level ridge exists on 17 May near northeastern China as shown by positive geopotential height anomalies. Under a surface high-pressure and light synoptic forcing, winds were generally light (e.g., 1–2 ms^{-1} observed at TRF) and westerly in the morning and afternoon, changing to calm winds at TRF after 14:00 KST. Based on the back-trajectory (Fig. 2), the light westerly winds in the morning transported pollutants from the western portion of the SMA to the eastern portion. As the flow became more quiescent in the afternoon, local emissions were pooled in the southeastern portion of the SMA and then continued directly into the rural forested area near TRF. This synoptic system also ushered in warm (24 and 27 °C at 15:00 KST at TRF and OLY, respectively)
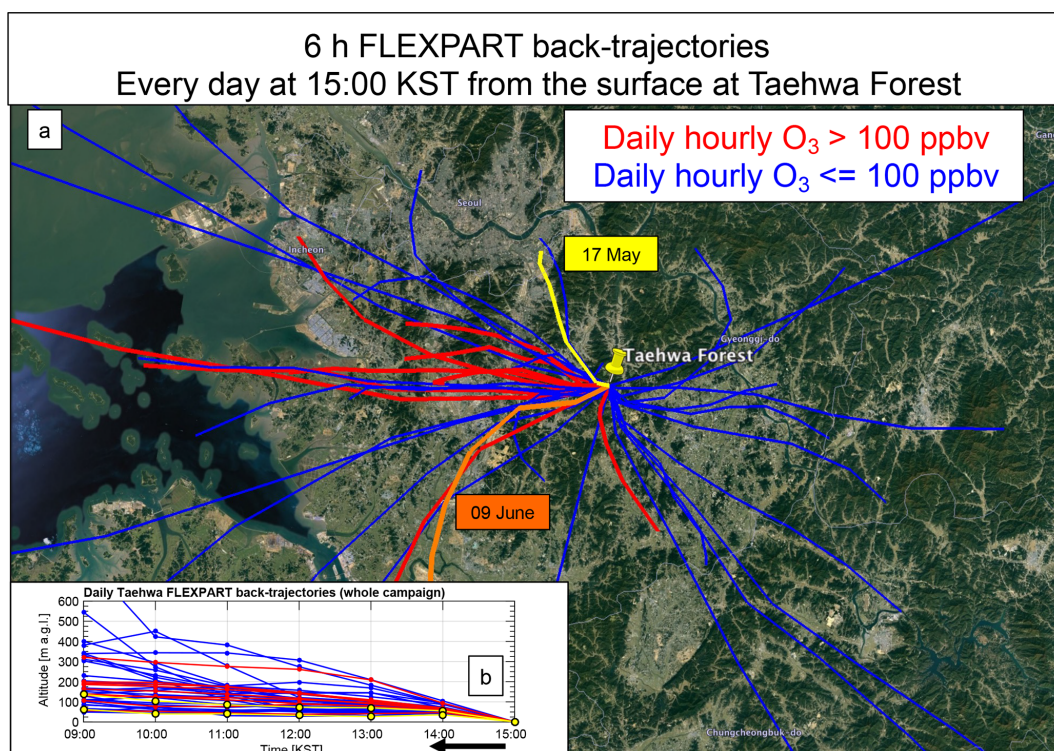
Figure 2. Daily 6 h FLEXPART back-trajectory **(a)** spatial and **(b)** vertical locations for all parcels initialized at 15:00 KST at TRF throughout the KORUS-AQ campaign. The two case studies are 17 May (yellow) and 9 June (orange).

and cloud-free conditions throughout the day. With this synoptic meteorology, unimpeded solar radiation, and ample O_3 precursor emissions from SMA, TRF reached a maximum hourly O_3 value of nearly 120 ppbv (Fig. 1d) at 17:00 KST, well above the 100 ppbv South Korean national standard.

In contrast, on 9 June a weak 500 hPa ridge existed over South Korea, the Yellow Sea, and eastern China with a +50 m height anomaly. Under this multi-day weak synoptic forcing, the back-trajectory indicates recirculation of the air mass throughout the Korean peninsula, rather than extended zonal transport. The air mass appears to have been tracked near Seoul on the previous day, followed by recirculation back to the densely forested region south and west of TRF. Light and northwesterly surface winds occurred in the morning and afternoon (e.g., 2–3 m s^{-1} at TRF), decreasing and becoming more southerly in the late afternoon (e.g., less than 0.5–1 m s^{-1} at TRF after 12:00 KST). Throughout the day, the light northwesterly transported pollutants from the northwest to the southeast within the SMA. As the flow reduced in the afternoon and became more southerly, local fresh (as well as aged and/or recirculated) emissions were pooled throughout the southern portion of the SMA, yielding adequate time to interact with the rural forested area near TRF. This system was also associated with much warmer (27 and 31 °C at 15:00 KST at TRF and OLY, respectively) conditions than those on 17 May, favoring increased emissions of BVOCs,

such as isoprene (Kim et al., 2015). With weakly forced synoptic meteorology, TRF reached a maximum hourly O_3 value of nearly 110 ppbv, exceeding the 1 h 100 ppbv South Korean national standard.

3   Case studies of pollution transport to TRF

3.1   Methods

Vertical profiles of key atmospheric chemical constituents measured via aircraft and from ground-based platforms (Table 1) during two representative case studies are used to better understand transboundary and local transport effects from urban regions to the rural landscape. To assess the transport and evolution of urban emissions impacting TRF, airborne measurements of O_3, NO_2, CO (carbon monoxide), SO_2 (sulfur dioxide), isoprene (C_5H_8), and toluene (C_6H_5-CH_3) were collected. Downwind plume chemistry is also further investigated and fingerprinted using the onboard DC-8 observations and an explicitly constrained 0-D photochemical box model simulation. Constituent profiles at TRF were also measured using ground-based instrumentation such as O_3 lidar (Sullivan et al., 2016, 2017), electrochemical cell (ECC) O_3 ozonesondes, and aerosol backscatter. Surface observations of O_3, NO_2, toluene, and isoprene at TRF are also presented.
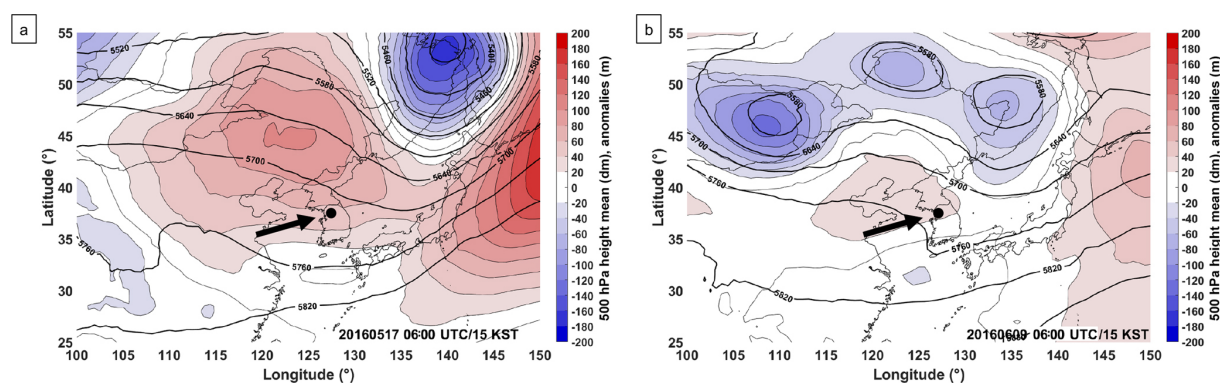
Figure 3. MERRA-2 500 hPa geopotential heights and anomalies for **(a)** 17 May and **(b)** 9 June 2016 at 21:00 KST (TRF marked in black dot/arrow).

Table 1. Measurement species divided by each platform used throughout the case studies.

Quantity	Method	Reference
Hanseo University King Air		
O_3	UV absorption, Teledyne T400	
NO_2	CAPS, Teledyne T500U	
CO	UV fluorimetry, AeroLazer (AL5002)	Kim et al. (2013)
SO_2	UV fluorimetry, Thermo 43i	
NASA DC-8		
O_3; NO_2	Chemiluminescence	Weinheimer (2006)
Isoprene, toluene	Proton-transfer-reaction time-of-flight mass spectrometer (PTR-TOF-MS)	Müller et al. (2014)
$P(O_3)$	0-D photochemical box model	Schroeder et al. (2016); (MCM v3.3, http://mcm.leeds.ac.uk/MCM/, last access: 27 March 2019)
NASA B-200 King-Air		
NO_2 slant column	GeoTASO	Nowlan et al. (2016)
Taehwa Research Forest (TRF)		
O_3	Lidar, UV differential absorption	Sullivan et al. (2014, 2015a, b)
O_3, temp., RH, winds	Electro-chemical cell, balloon-borne	Thompson et al. (2007, 2019); Witte et al. (2017)
O_3	UV absorption, Thermo 49i	https://www.thermofisher.com/order/catalog/product/49I (last access: 27 March 2019)
NO_2	CAPS, Teledyne T500U	https://www.epa.gov/research (last access: 28 March 2019)
Atm. backscatter	Vaisaila CL-51	https://www.epa.gov/research (last access: 28 March 2019)
Isoprene, toluene	Proton-transfer-reaction mass spectrometer (PTR-ToF-MS)	Kim et al. (2010)

The instruments aboard the NASA DC-8 and Hanseo University King Air provide accurate, fast-response measurements of trace gases and can be used in conjunction with aircraft-based remote sensing instruments in some cases to extend the characterization of pollution events. The Geostationary Trace gas and Aerosol Sensor Optimization (Geo-TASO) airborne instrument was aboard the NASA B-200 King Air performing push broom raster sample routes to complement flights. Measurements of backscattered solar radiation are used to determine slant column (slcol) amounts of NO_2 at $250\,\text{m} \times 250\,\text{m}$ spatial resolution, providing a quantitative spatial distribution of NO_2 throughout the SMA.

Ozonesonde profiles at TRF

A total of 34 O_3 ozonesondes were released from TRF throughout KORUS-AQ from 10 May to 12 June. Afternoon soundings (31 of the 34 launches between 13:30 and

16:30 KST) of O_3 (Fig. 4a) and temperature (Fig. 4b) illustrate day-to-day variability in the first 3 km a.s.l. From 10 to 16 May, concentrations were mostly between 70 and 80 ppbv, which were associated with cooler temperatures and higher synoptic wind speeds. However, by the early afternoon of 17 May, a stagnant high-pressure system located over the Yellow Sea (see Fig. 3a) introduced a warmer air mass, calmer winds, and clearer skies. Through most of the campaign until 3 June, a similar meteorological setup persisted, providing favorable conditions for rapid O_3 production to more than 120 ppbv. On 4 and 6 June, intermittent shower activity events limited O_3 production. However, by 9–10 June another high-pressure system (see Fig. 3b) approached the region, increasing temperatures, suppressing wind speeds, and fostering O_3 build-up. Two case studies (17 May; 9 June, black boxes) are presented in this section and Fig. 4 emphasizes the regularity of these enhanced levels of pollution.

A box-and-whisker plot of the O_3 profiles binned in 500 m layers is also shown in Fig. 4. There were large disparities in boundary layer O_3 throughout the campaign period as compared to free tropospheric conditions. Within the first 2 km, median, lower quartile, and upper quartile ranges were 76–95, 67–76, and 87–108 ppbv, respectively. There were no outliers within this altitude region, indicating the sondes were consistently sampling increased pollution events on flight and non-flight days during the campaign. Within the free troposphere from 2 to 6 km, median and lower quartile O_3 values were from 73 to 81 and 66 to 74 ppbv, respectively. This is markedly larger than the 50–65 ppbv baseline O_3 estimates derived for Trinidad Head, CA; Boulder, CO; and Huntsville, AL, USA (Stauffer et al., 2016; Kuang et al., 2017). This highlights the infrequency (i.e., < 25 % of the time) of measuring less than 66 ppbv of O_3 within the boundary layer and free troposphere and the subsequent regulatory challenge of meeting the 8 h Korean O_3 standard (60 ppbv).

3.2 Pollution event: 17 May 2016

3.2.1 Aircraft analyses: Hanseo University King Air

The positioning of the large-scale ridge displayed in Fig. 3a was favorable for transport of Chinese industrial (e.g., CO; SO_2) and urban emissions to the Korean peninsula (Lee et al., 2008). To assess potential transboundary transport from other East Asian megacities, trajectories are shown for a full 48 h prior to reaching TRF at 17 May at 15:00 KST. The 48 h back-trajectory (top panel, Fig. 5) indicates the air mass was transported over the eastern China province of Shangdong, the Yellow Sea, and SMA prior to reaching TRF. Pollution entering South Korea via this pathway was measured by NIER instruments (Table 1) aboard the Hanseo University King Air aircraft during the morning of 17 May 2016 (Fig. 5).

The Hanseo University King Air conducted a sampling pattern that included a near-ground-level approach in Seoul and westbound leg out towards the Yellow Sea (green panel, Fig. 5), a southbound leg directly over the Yellow Sea at two altitudes (orange panel, Fig. 5), a returning eastbound leg (magenta panel, Fig. 5), and then finally a northbound returning leg towards Seoul (cyan panel, Fig. 5). During this pattern, measurements of O_3, NO_2, CO, and SO_2 capture long-range pollution transport across the Yellow Sea. Eastern China is densely populated with coal-fired power plants, which are strong emitters of NO_x, SO_2, and particulate matter (Zhao et al., 2008). Carbon monoxide and SO_2 are longer lived species with lifetimes on the order of 1–2 months (Miyakazi et al., 2012) and 1–2 days (He et al., 2012), respectively, and are used to support the interpretation of transboundary pollution transport. During the KORUS-AQ study period, Huang et al. (2018) has further used CO to evaluate chemical transport models and assess transboundary impacts on the Korean peninsula.

During the low-level approach to Seoul near 08:55 KST (denoted with dashed black line, Fig. 5) chemical sampling of low O_3 (20–40 ppbv), high NO_2 (20–40 ppbv), high CO concentrations (500–700 ppbv), and high SO_2 (6–10 ppbv) are observed in the first 500 m a.s.l. These indicate morning urban emissions (and subsequent O_3 titration) and because of the proximity to the surface level, these pollutants are largely associated with local SMA vehicular and industrial morning emissions. As the aircraft moves westward at 1000 m a.s.l., it samples a much cleaner air mass but reaches a plume of polluted air near 09:20 KST, associated with increased concentrations of O_3 (to 90 ppbv), CO (to 500–600 ppbv), and SO_2 (to 6–8 ppbv). In conjunction with the 48 h back-trajectory, this is likely the outflow of aged industrial emission from eastern China (Zhao et al., 2008) that has been transported over the Yellow Sea. Similar concentrations of these species are observed during the southbound leg at 500 m a.s.l., indicating that the vertical distribution of pollutants is relatively well mixed in the polluted air mass from 500 to 1000 m a.s.l. During the eastbound leg at 1500 m a.s.l., the aircraft samples mostly clean air with the exception of a pollution plume at 10:55 KST. As the aircraft returns to the Korean peninsula, it observes relatively cleaner conditions until it approaches the southern portion of the SMA near 11:30 KST.

In summary, the westbound in situ observations indicate transport of polluted air across the Yellow Sea towards South Korea. The largest chemical perturbations (e.g., 15–40 ppbv in NO_2; 6–10 ppbv in SO_2, 200–300 ppbv in CO) during the flight pattern were spatially correlated with local emission sources during the initial ground level approach and the final transect nearing the SMA. The southbound transect indicated on this day that the background level of O_3 is near 60 ppbv and a 20–30 ppbv enhancement in O_3 is observed at 500 m over the water. However, the increases in NO_2 are chemically responsible for rapid O_3 production, which were observed in near-negligible amounts during the transboundary transects.
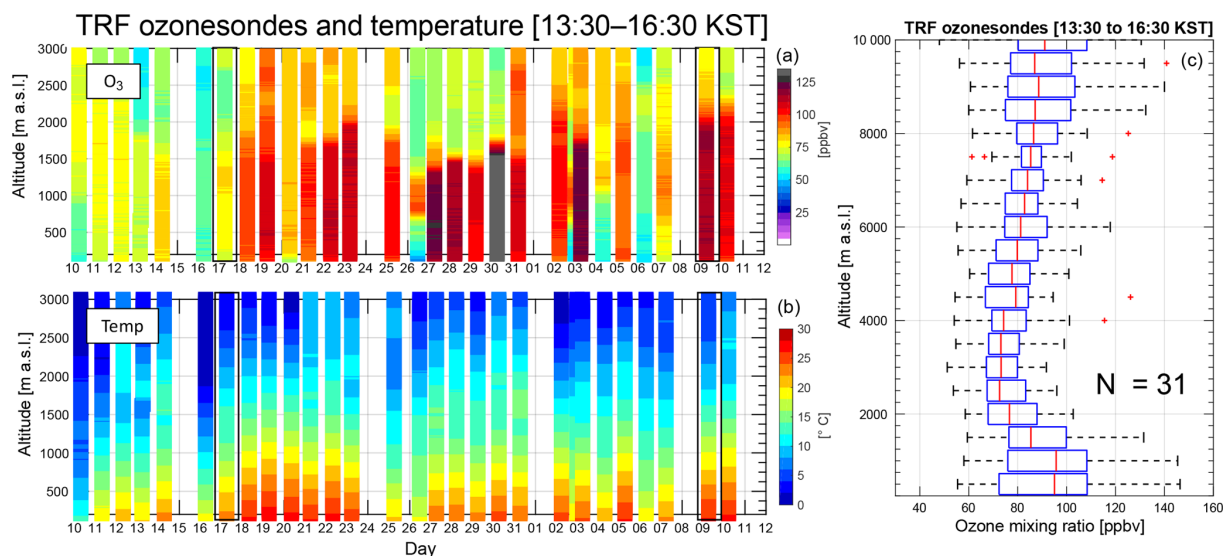
Figure 4. Afternoon soundings (13:30 to 16:30 KST) of O_3 (**a**, from ECC O_3 ozonesondes) and temperature (**b**, from concurrent radiosondes) and a box-and-whisker plot (**c**) illustrate day-to-day variability at TRF. The two case studies (17 May and 9 June) are highlighted with black boxes.

3.2.2 Aircraft analyses: NASA DC-8

Chemical observations from the NASA DC-8 throughout the SMA from 15:05 to 15:40 KST on 17 May 2016 are presented (Fig. 6). The aircraft route (Fig. 6a, with arrows) begins in the southern region at 2.1 km a.s.l., moving northwards towards TRF and descending to near 1.7 km a.s.l. The aircraft maintains this altitude on a northward track and turns westward and descends to near 1.0 km a.s.l. towards Seoul to perform a near-ground-level pass near the Seoul Incheon airport. The aircraft continues at 1.0 km a.s.l., overpasses TRF near 0.5 km a.s.l., descends to nearly 0.3 km a.s.l., and then quickly ascends out of the boundary layer. The constituents shown from the flight path are O_3 (Fig. 6b), NO_2 (Fig. 6c), isoprene (Fig. 6d), toluene (Fig. 6e), and O_3 production ($P(O_3)$, Fig. 6f).

Toluene, a reactive aromatic and industrial VOC, is a useful tracer for urban anthropogenic emissions because it is a highly reactive O_3 precursor with a chemical lifetime on the order of a day. Toluene is a dominant VOC throughout the SMA and contributes to nearly 60.7 % of the total VOC emissions (Lee et al., 2011). Isoprene, a BVOC and derivative of photosynthesis, is largely associated with deciduous trees (e.g., oak, which accounts for 85 % of broadleaf trees in South Korea; Lim et al., 2011). Isoprene can enhance photochemical O_3 production, is emitted almost entirely during the daytime, can form additional oxidative byproducts, and is released more abundantly with increased temperatures. Previous results from Kim et al. (2015) indicate that isoprene accounts for most of the midday hydroxyl radical (OH) reactivity (11:00–15:00 KST) at TRF and can rapidly increase O_3 production rates.

Within the SMA and below 0.5 km a.s.l., there is a significant chemical perturbation as compared to the free tropospheric concentrations of NO_2 (40–50 ppbv, Fig. 6c) and toluene (5–7 ppbv, Fig. 6e). These increases both lead to increases in modeled $P(O_3)$ (10–20 ppbv h^{-1}, Fig. 6f). Isoprene is mostly less than 0.3 ppbv during this sampling. The concentrations of NO_2 have increased by 10–20 ppbv since the afternoon Hanseo University King Air sampling (Fig. 5), indicating a persistent reservoir of reactive nitrogen coming from SMA throughout the day. Additional DC-8 observations (not shown) indicate NO_2 accounted for 70 %– 90 % of the total reactive nitrogen during the 17 May overpass at TRF. Ozone remains mostly between 70 and 80 ppbv (Fig. 6b) during the initial descent into Seoul, indicating emissions are fresh enough that rapid O_3 production has not occurred yet (which is further corroborated with the $P(O_3)$ model output).

As the aircraft moves towards TRF, it samples various spatial chemical gradients. For example, NO_2 and toluene concentrations decrease to near 20–30 ppbv and near 2–3 ppbv, respectively. An increase in isoprene concentrations to 0.5– 0.8 ppbv corresponds to the forested region southeast of Seoul. Directly over TRF, O_3 concentrations are increased as compared to those near Seoul by 5–10 ppbv, indicating that downwind O_3 production has increased with diluted levels of NO_x. The aircraft passes TRF and continues its eastward descent to 0.3 km a.s.l.; O_3 concentrations markedly increase to between 110 and 125 ppbv and $P(O_3)$ rapidly increases to between 20 and 32 ppbv h^{-1}. Although the aircraft samples nearly negligible concentrations of isoprene and NO_2, toluene concentrations have increased and are comparable to those sampled near Seoul (3–4 ppbv). This is a strong indica-
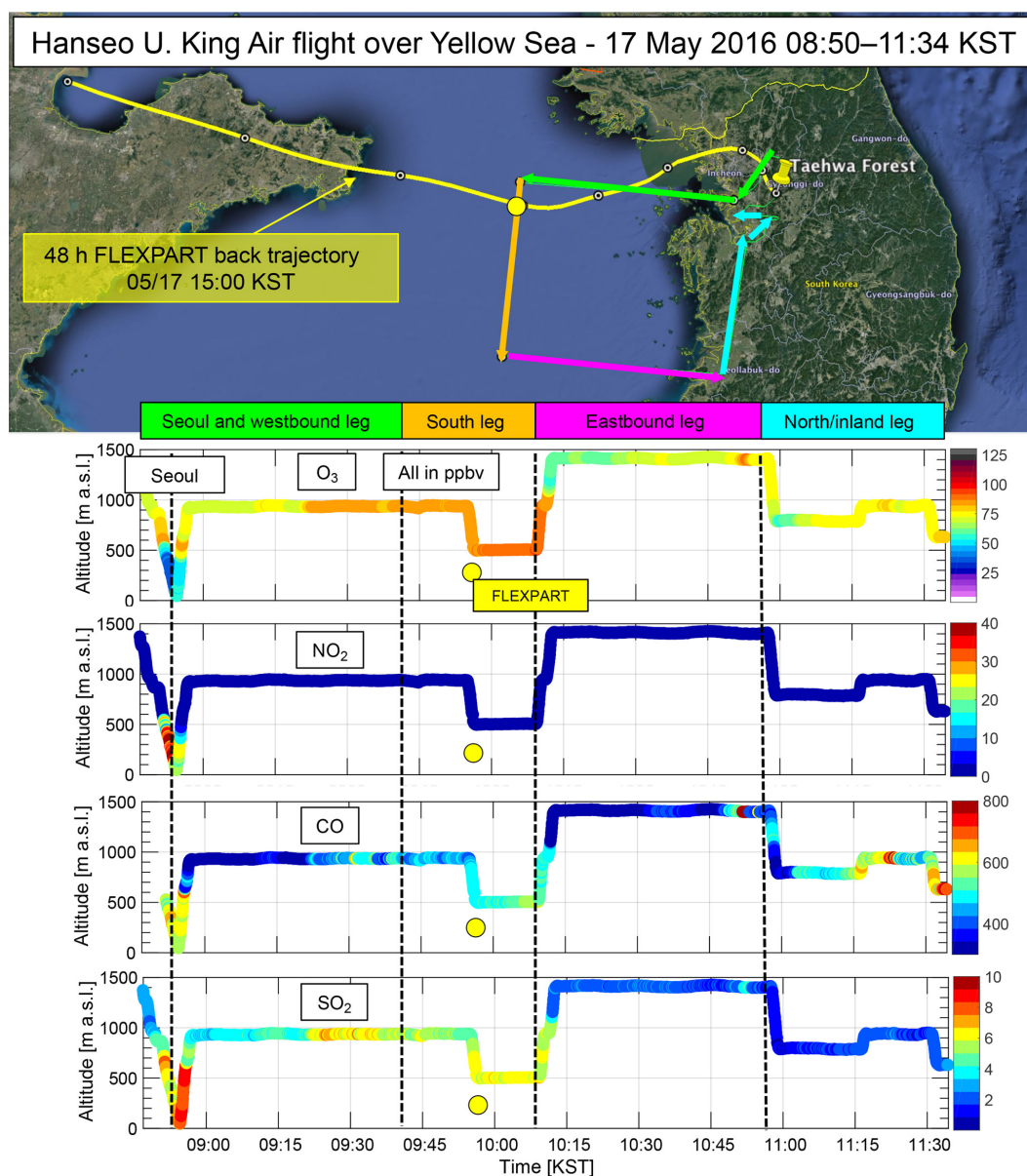
Figure 5. Hanseo University King Air Flight on 17 May 2016 to sample O_3, NO_2, CO, and SO_2 over South Korea and the Yellow Sea from 08:50 to 11:34 KST. The 48 h FLEX-PART back-trajectory, which was initialized at 15:00 KST on 17 May 2016, is also shown.

tor of an aged urban air mass containing highly reactive O_3 precursors impacting rural sites. In summary, transboundary pollution transport was observed via the Hanseo University King Air (Fig. 5) on 17 May, but locally emitted O_3 precursors can be confidently attributed as a catalyst for the highest levels of boundary layer O_3 production observed near TRF.

3.2.3 Ground-based observations at TRF

To fingerprint and quantify the transported pollution reaching TRF, diurnally resolved observations are presented in Fig. 7 for the entirety of 17 May.

08:00 to 12:00 KST. Ceilometer observations (Fig. 7a) and GSFC O_3 lidar observations (Fig. 7b), both containing an aerosol mixing height retrieval (black line), indicate residual layers and vertical stratification. Above the boundary layer between 1000 and 1700 m a.s.l., enhanced aerosol backscatter and concentrations of O_3 near 70–80 ppbv are similar in concentration and altitude to the transboundary pollution observed during the morning Hanseo University aircraft flight (Fig. 5). Atmospheric layering also exists below 850 m a.s.l., with a distinct high O_3 (100–120 ppbv) region near 600 m a.s.l. and low O_3 (20–40 ppbv) and high aerosol backscatter from 600 to 850 m a.s.l. Although NO_2 concen-
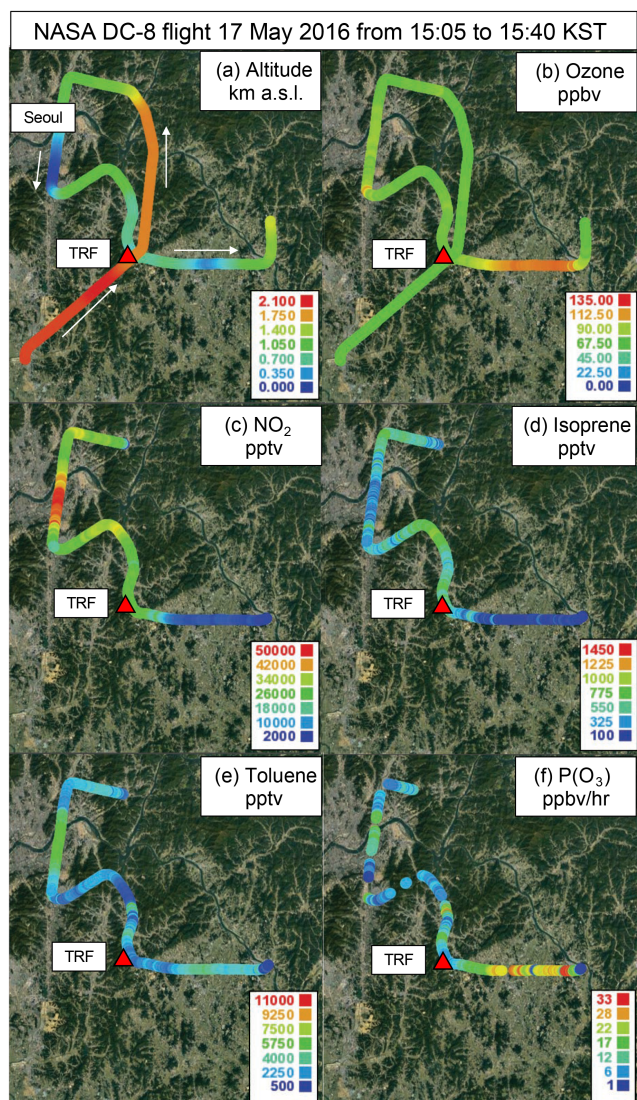
Figure 6. NASA DC-8 measurements of **(a)** altitude, **(b)** O_3, **(c)** NO_2, **(d)** isoprene, **(e)** toluene, and **(f)** modeled $P(O_3)$ from the afternoon science flight on 17 May 2016 from 15:05 to 15:40 KST. Seoul and TRF are denoted.

similar chemical composition to the plume observed "downwind", or east, of TRF in the DC-8 observations, indicating O_3 production continued as it moved away from the SMA. O_3 concentrations begin to decrease (by 25 ppbv) near 14:00 KST, in conjunction with a 25 ppbv increase in NO_2, conserving total odd oxygen (O_x). Near 15:20 KST, the DC-8 overflew TRF and sampled comparable concentrations of O_3 and NO_2 as the lidar, sonde, and surface measurements. As emissions continue to photochemically process and advect over the TRF site, there is a rapid increase in O_3, well-mixed throughout the boundary layer, at TRF between 16:00 and 17:00 KST. Ozone concentrations increase by 60 ppbv and NO_2 decreases by 15 ppbv, indicating total O_x is not conserved and a passing plume of urban emissions has arrived at TRF. Isoprene (Fig. 7d) does not show a rapid change throughout the day; however, it is near peak concentration during this time. Concentrations of O_3 above 125 ppbv persist until 18:30 KST, although the mixing height decreases rapidly during this time. The in situ observations indicate concentrations were above 100 ppbv until 18:30, indicating polluted conditions persisted well into the evening at the surface and even longer aloft. This later afternoon buildup and transport is also identified with results from Lennartson et al. (2018) during the KORUS-AQ study, which indicate TRF had consistently higher aerosol optical depth (AOD) values of near 0.4–0.6 in the morning, decreasing throughout the day and eventually rising again in the early evening at 15:00–16:00 KST.

19:00–23:00 KST. After sunset (near 19:00 KST), increases in aerosol backscatter and O_3 near 1500 m a.s.l. are observed, indicating a stable residual layer persisted into the evening, trapping pollutants at TRF. As surface O_3 quickly decayed to near 20 ppbv after 19:00 KST, it corresponded to increases in NO_2 from near 15 to 20–30 ppbv and toluene from 2 to 4 ppbv, which corroborate the incoming pollution plume quantified with the DC-8 observations (Fig. 6c, e). This indicates TRF was continuously perturbed by local urban emissions into the evening hours and this has likely affected the next day's chemical composition (e.g., Fig. 4 indicates O_3 at TRF on 18 May exceeded > 100 ppbv). Although the combined suite of aircraft (Fig. 5) and lidar and ceilometer observations (Fig. 7a, b) suggest transboundary O_3 and pollutants reached the TRF site, the lidar and in situ observations clearly indicate domestic anthropogenic emissions were the dominant source of the O_3 exceedance at TRF.

3.3 Pollution event: 9 June 2016

3.3.1 Aircraft analyses: NASA DC-8

Chemical observations were made with the NASA DC-8 instruments in a similar pattern to those on 17 May 2016 throughout the SMA from 15:20 to 15:55 KST on 9 June 2016 (Fig. 8a, with arrows). However, the aircraft remained at lower altitudes during the flight pattern prior to
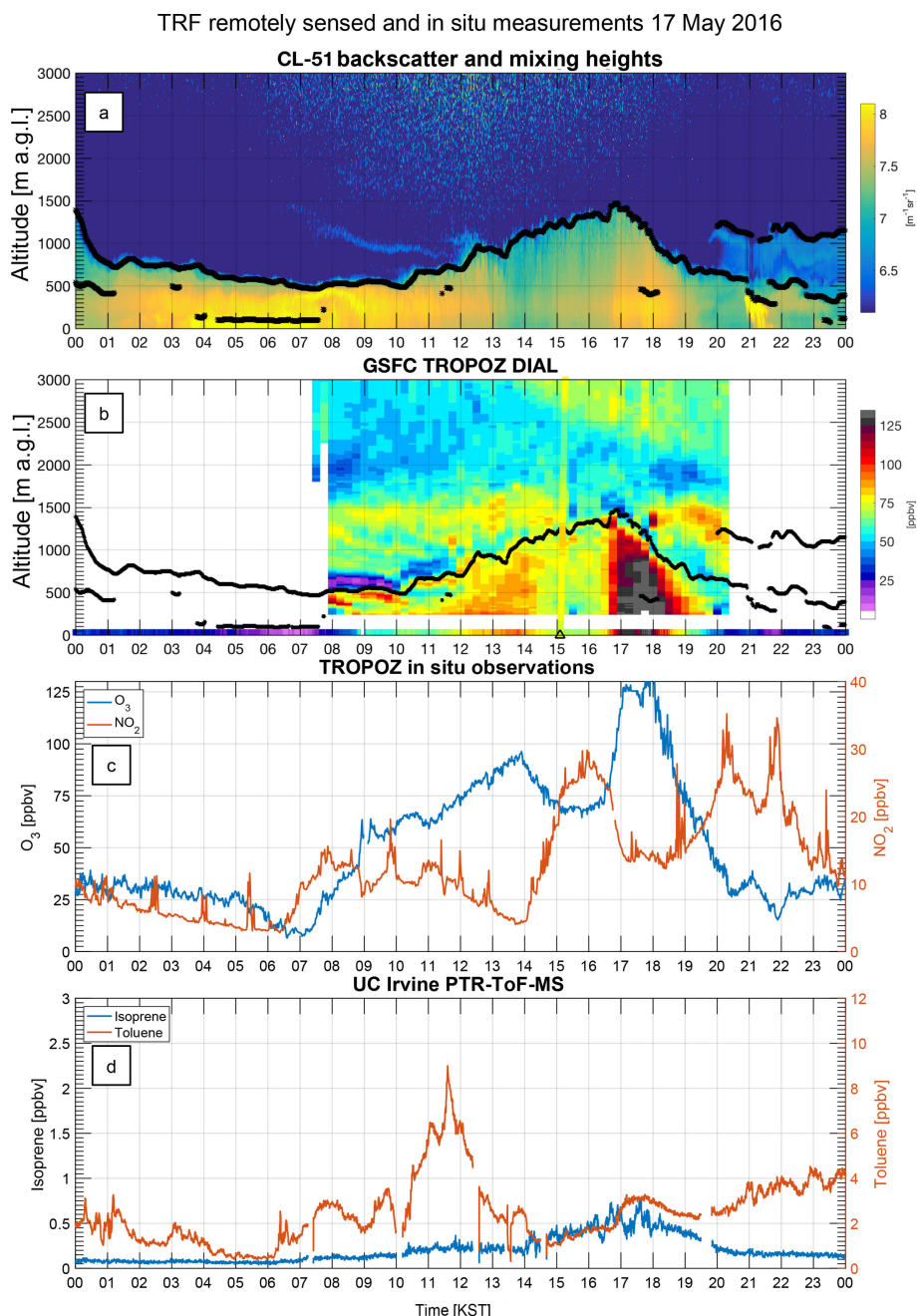
trations are enhanced from 5 to 15 ppbv during this segment, near 09:00 KST, residual layer entrainment appears to occur as surface O_3 (Fig. 7c) abruptly increases from 40 to 60 ppbv. Increases in nitrate aerosol, either through N_2O_5 hydrolysis or morning residual layer entrainment, within the SMA during the KORUS-AQ study have been further examined by Kim et al. (2018). Near 11:30 KST, toluene (Fig. 7d) levels increase to peak values for the day, near 8–9 ppbv, indicating the transport of urban industrial emissions (including the increased NO_2) to the site is well underway.

12:00 to 19:00 KST. The boundary layer is convectively well-mixed to 1200 m a.s.l. with O_3 concentrations near 85–95 ppbv, similar to the in situ surface monitor. This plume has

Figure 7. Time series of **(a)** ceilometer backscatter profiles and mixing heights, **(b)** GSFC TROPOZ DIAL O_3 profiles, **(c)** in situ surface O_3 and NO_2, and **(d)** isoprene and toluene concentrations for 17 May 2016. Note: the DC-8 overpass occurred at around 15:30 KST. The colocated ozonesonde is denoted in **(b)** with a black triangle.

the initial upper-level pass of TRF. This resulted in low-level sampling of the forested region and recirculated air mass. This aged air mass was associated with increased concentrations of O_3 to over 120 ppbv (Fig. 8b), low concentrations of NO_2 (less than 5 ppbv; Fig. 8c), variable concentrations of toluene (between 5 and 10 ppbv; Fig. 8e), variable concentrations of isoprene (between 0.1 and 0.7 ppbv; Fig. 8d), and $P(O_3)$ values between 20 and 35 ppbv h^{-1} (Fig. 8f).

As the aircraft ascended out of the boundary layer prior to reaching Seoul, O_3 remained above 100 ppbv near 2000 m a.s.l. Mixing heights are 500 m deeper than on 17 May, presumably as a result of warmer temperatures and greater convective mixing. As the DC-8 ascended out of the overpass south of Seoul, NO_2 concentrations reached 20–30 ppbv, toluene reached 3–6 ppbv, and isoprene exceeded 1.2 ppbv (nearing the peak concentration measured via the
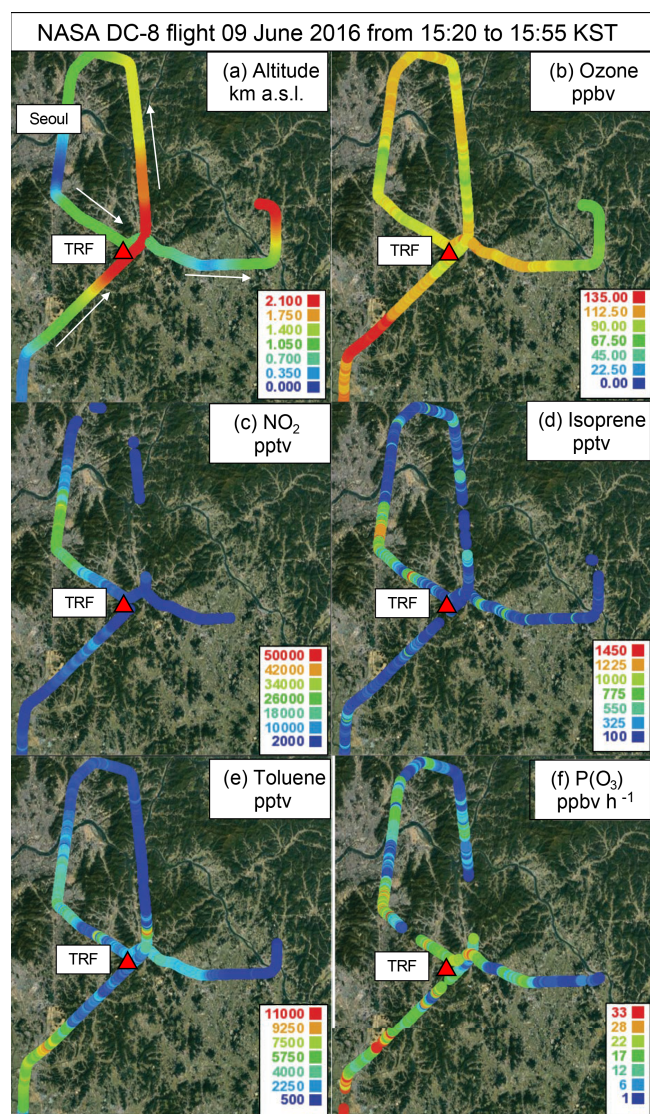
Figure 8. NASA DC-8 measurements of **(a)** altitude, **(b)** O_3, **(c)** NO_2, **(d)** isoprene, **(e)** toluene, and **(f)** modeled $P(O_3)$ from the afternoon science flight on 17 May 2016 from 15:05 to 15:40 KST.
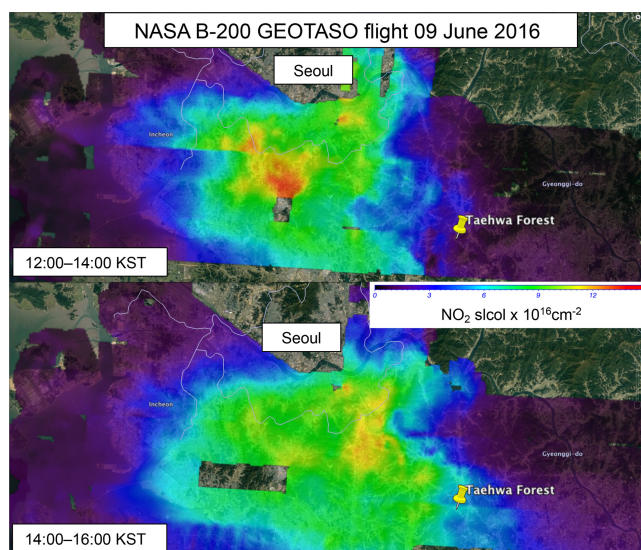

Figure 9. Observations of NO_2 slant columns from the GeoTASO instrument during the two afternoon science flights on 9 June 2016 from 12:00 to 14:00 and 14:00 to 16:00 KST. TRF and Seoul are denoted.

3.3.2　Aircraft analyses: NASA B-200

On 9 June 2016, the NASA B-200 performed a morning and afternoon raster (Fig. 9) of the greater SMA from 12:00 to 14:00 and 14:00 to 16:00 KST, respectively. This yields a unique view of the concentrations and chemical transport of NO_2 throughout the SMA during the afternoon hours. During the 12:00–14:00 KST sampling, there is a clear maximum in NO_2 slant columns in the south and west of Seoul. Afterwards, the 14:00–16:00 KST measurements show the advection of NO_2 (and presumably other urban pollutants) eastward and southward throughout the SMA. During the 14:00–16:00 flight, large NO_2 column amounts extend to the southeastern portion of the SMA, with enhanced levels of NO_2 reaching the edge of TRF.

3.3.3　Ground-based observations at TRF

To fingerprint and quantify the chemical transport reaching TRF, diurnally resolved observations are presented in Fig. 10 for the entirety of 9 June.

08:00 to 12:00 KST. Similar to 17 May, vertical profiles of aerosol backscatter and O_3 (Fig. 10a, b) throughout 9 June indicate residual layering of the atmosphere in the morning hours. There exist descending layers of aerosols above the residual layer associated with the recirculation of the air mass from the previous day. Near 09:00 KST entrainment of the residual O_3 corresponds to an abrupt surface O_3 increase from 20 to 55 ppbv (Fig. 10c). TRF is impacted with increased surface NO_2 (Fig. 10c) towards 30 ppbv and toluene (Fig. 10d) towards 4 ppbv during this time. Warmer temper-
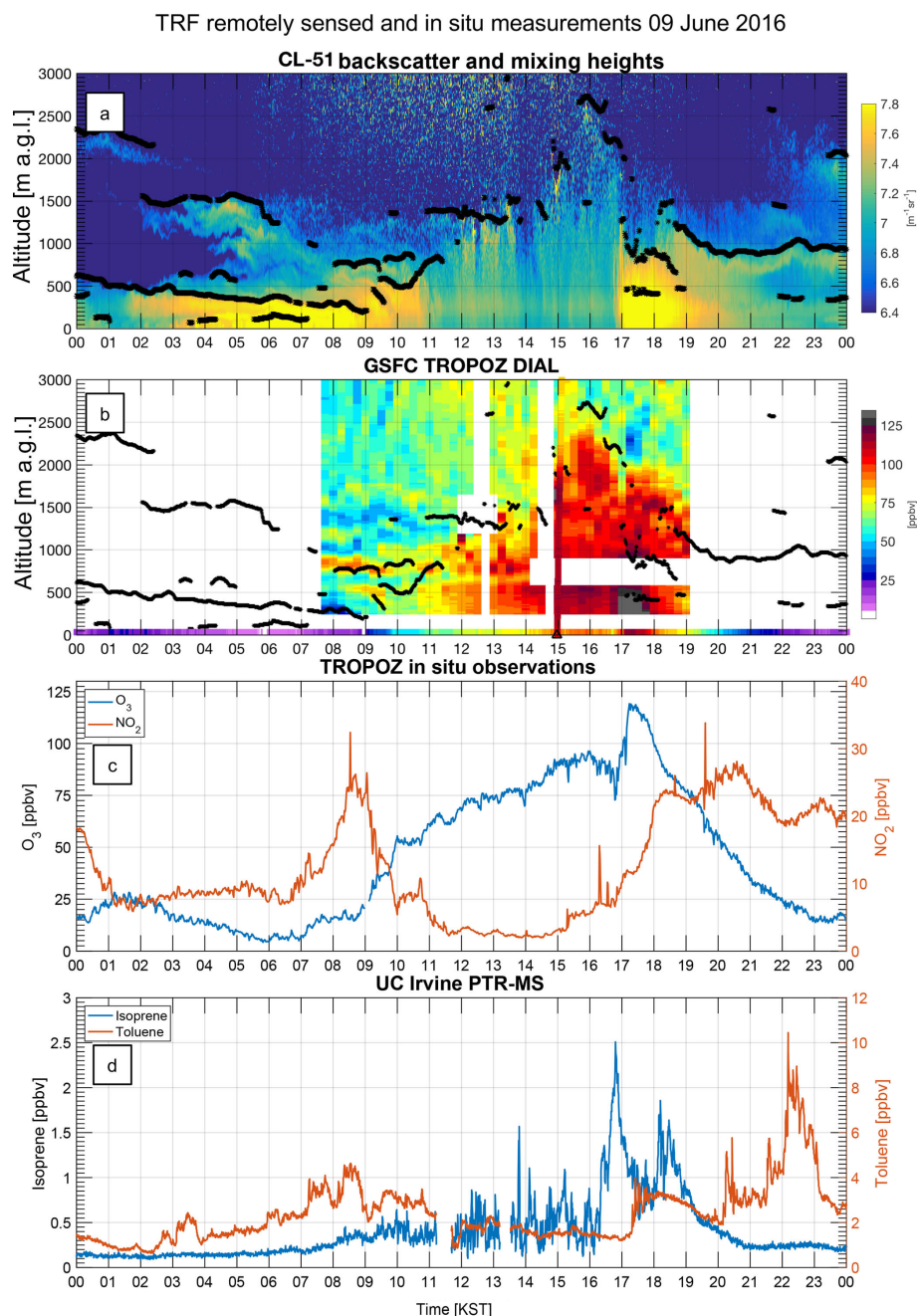
DC-8 during the entire campaign). This air mass was also associated with lower values of O_3 and $P(O_3)$ as compared to the forest plume south of TRF, at 75–90 ppbv and 10–20 ppbv h^{-1}, respectively, indicating the anthropogenic and biogenic emissions were still fresh. Similar to 17 May, as the aircraft leaves urban Seoul and approaches TRF there is a strong spatial gradient in nearly all chemical constituents. At TRF, O_3 and $P(O_3)$ increase to over 120 ppbv and 30 ppbv h^{-1}, respectively, while NO_2 decreases to 5–10 ppbv, indicating O_3 production was rapidly occurring and impacting rural sites downwind of Seoul.

TRF remotely sensed and in situ measurements 09 June 2016

Figure 10. Time series of **(a)** ceilometer backscatter profiles and mixing heights, **(b)** GSFC TROPOZ DIAL O_3 profiles, **(c)** in situ surface O_3 and NO_2, and **(d)** isoprene and toluene concentrations for 9 June 2016. Note: the DC-8 overpass occurred near 15:30 KST. The colocated ozonesonde is denoted in **(b)** with a black triangle.

atures on 9 June compared to 17 May lead to higher daytime isoprene concentrations (0.5 vs. 0.3 ppbv).

12:00 to 19:00 KST. Boundary layer concentrations of O_3 and aerosols are well mixed with steady growth in O_3 from 12:00 until 16:30 KST, when a rapid influx of O_3 and aerosol occurs. This occurs after a significant positive perturbation in isoprene and precedes an abrupt increase in NO_2 and toluene. The O_3 peak closely corresponds to the O_3 sampled via the

DC-8 south and west of TRF, and in conjunction with the back-trajectory (Fig. 2), it appears O_3 was likely advected through TRF during this time.

19:00 to 23:00 KST. As solar radiation declines, in-air concentrations of O_3 near 100 ppbv mixing to 2000 m a.s.l. are observed, indicating a stable residual layer persisted into the evening and likely impacted the next day's O_3 composition (e.g., Fig. 4 indicates O_3 at TRF on 10 June ex-
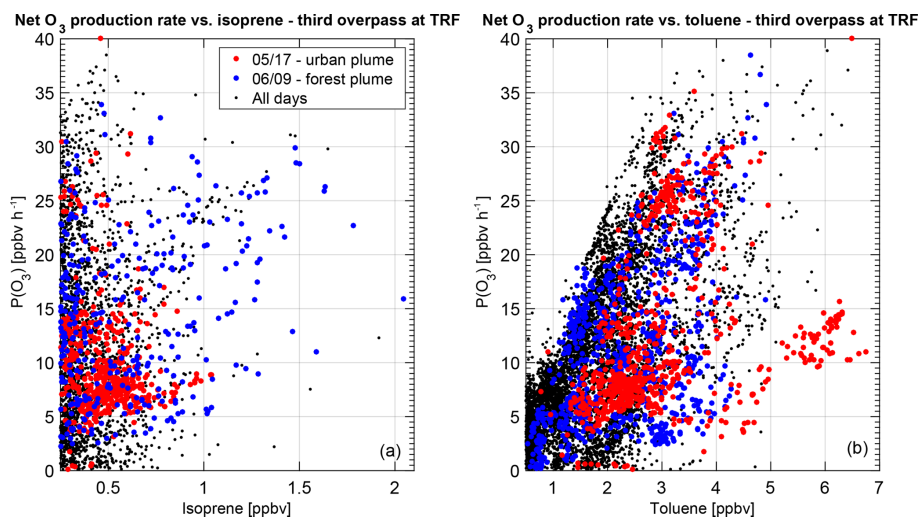
Figure 11. Photochemical model output of net O_3 production, $P(O_3)$, for all afternoon flights during the KORUS-AQ study compared to measured concentrations of isoprene (**a**) and toluene (**b**). The case studies described in Sect. 3 are denoted in red (17 May 2016) and blue (9 June 2016).

ceeded > 100 ppbv). As surface O_3 quickly decayed to near 20 ppbv after 19:00 KST, it corresponded to increases in NO_2 from near 15 to 20–30 ppbv and toluene from 8 to 10 ppbv, which points to the incoming pollution plume captured with the GeoTASO observations (bottom panel, Fig. 9), indicating TRF was impacted by regional urban emissions into the evening hours. In conjunction with the aircraft, lidar, and surface in situ observations, this case study emphasizes the role of domestically produced emissions (both biogenic and anthropogenic) in perturbing the chemical composition downwind of Seoul.

4   Case studies in the context of the entire KORUS-AQ study

4.1   Aircraft observation and $P(O_3)$

Although two case studies are presented to illustrate the contrasting types of pollution influences at TRF, it is important to assess how representative events were for the entire KORUS-AQ study. To do this, the chemical observations of isoprene (Fig. 11a) and toluene (Fig. 11b) aboard the NASA DC-8 are presented for all remaining afternoon flights (exact dates can be found here: http://www-air.larc.nasa.gov/missions/korus-aq/, last access: 27 March 2019). Data were used when the DC-8 aircraft was below 1.5 km a.s.l. within 1° latitude and longitude of the TRF site. They are compared with the photochemical box model results in order to illustrate the relative contribution of VOCs and BVOCs on O_3 production during the campaign. In both panels of Fig. 11, the case studies chosen (17 May – red, 9 June – blue) appear to be accurate representations of "typical" pollution events seen at TRF as recorded by all other days (black dots).

For isoprene, 17 May had concentrations centered around 0.5 ppbv and were associated with $P(O_3)$ values between 5 and 15 ppbv h^{-1}. However, 9 June concentrations of isoprene were well over 0.5 ppbv, extending to over 2.0 ppbv. These were associated with $P(O_3)$ values in excess of 20 ppbv h^{-1} and nearing 35 ppbv h^{-1}, indicating that biogenic emissions contributed more to net O_3 production on this day than on 17 May. The 9 June case yielded nearly the highest isoprene-driven O_3 production rates during the campaign.

For toluene, 17 May appears to have several focused regions of toluene nearing 7 ppbv mostly associated with $P(O_3)$ at or below 15 ppbv h^{-1}. However, there is a subset of toluene with concentrations between 3 and 5 ppbv that are associated with $P(O_3)$ rates between 20 and 35 ppbv h^{-1}. This is indicative of the aged urban plume associated with O_3 photolysis reaching the area east of TRF. On 9 June, concentrations of toluene are nearly all below 5 ppbv and are grouped much closer together. This is indicative of a much more well-mixed air mass (which was also suggested with the Geo-TASO observations). Although 9 June was associated with a larger contribution of isoprene-driven O_3 production, it had a similar concentration of toluene to 17 May, indicating that both contrasting high-pollution events (and $P(O_3)$) were associated with high levels of urban pollutants.

4.2   GSFC O_3 lidar-derived campaign average

NASA GSFC O_3 lidar profiles at TRF during all flight days during the KORUS-AQ campaign (Fig. 12) can be used to derive a diurnal campaign average (see Sullivan et al., 2015c). The early morning low O_3 feature is prominent in the composite figure, as well as the in-air residual O_3 concentrations we have linked to transboundary transport between 65 and 75 ppbv above 500 m a.s.l. As solar radiation and
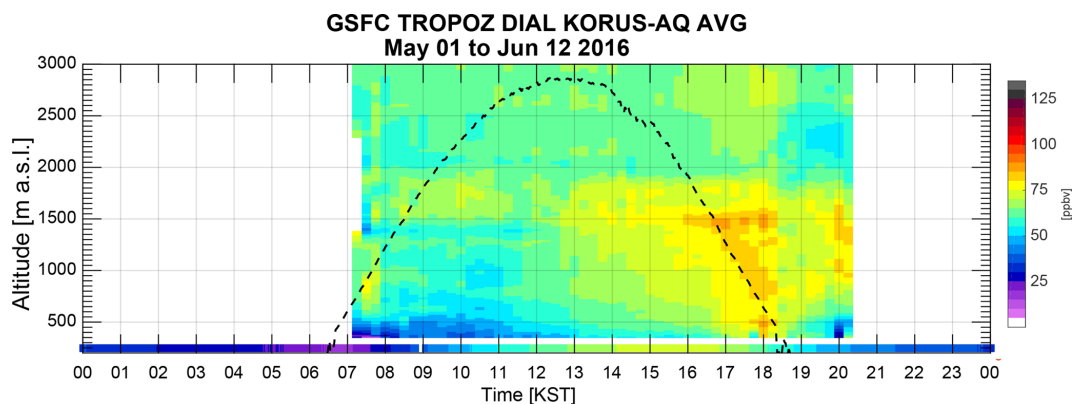
Figure 12. Composite averaged curtain of GSFC TROPOZ DIAL observations during the KORUS-AQ study period. This comprises 31 days of lidar data and over 250 h of measurements averaged together, and the analogous surface measurements and solar curve proxy are also overlaid.

convective mixing increase in the late morning hours (after 11:00 KST), surface concentrations of O_3 correlate better with concentrations measured aloft from the lidar. In the afternoon hours, O_3 increases at a rate of 5 ppbv h^{-1} between 500 and 1500 m a.s.l. and peak O_3 is observed between 17:00 and 18:00 KST. The difference between in-air and surface concentrations in the evening can be linked to a decoupling of the surface layer and rapid depletion and titration of surface O_3 from local NO_x emissions. This process isolates the polluted in-air residual layer during nighttime hours that will potentially affect downwind locations on the following morning. This confirms that during the May–June time period, the late-day peak O_3 occurrence is a persistent feature and is more enhanced than at the surface.

5   Conclusions

As part of the KORUS-AQ study, nearly continuous chemical measurements at the surface and within the first 3 km a.s.l. have quantified several of the key pollution features (e.g., residual layer O_3 entrainment and late-day O_3 maxima) responsible for O_3 exceedances observed at a rural site downwind of Seoul. The combination of aircraft (NASA DC-8, Hanseo University King Air, and NASA B-200), in situ (surface level and balloon-borne) and remotely sensed (O_3 lidar, ceilometer) measurements, in conjunction with photochemical model simulations, have produced significant findings about the origins of pollution reaching TRF that appear to be representative of other rural sites in South Korea. Two detailed case studies have been presented, which indicate a mixture of urban–anthropogenic emissions and biogenic emissions impacting TRF. These case studies are also characteristic of the entire study (see Fig. 12), suggesting late-day O_3 increases occur frequently at TRF, and that rural sites in this region may be experiencing long-term negative effects of O_3. Because threshold health effects, mortality rates,

and crop yield analyses have been historically calculated using only surface measurements (Lee et al., 2000; Kim et al., 2004; Wang and Mauzerall, 2004; Ghim et al., 2000), Fig. 12 also indicates that these analyses may be underestimating the extent of the negative impacts of high O_3 at TRF and its surrounding rural areas.

These results clearly demonstrate that Korea is subject to highly (aged) polluted air masses that cross the Yellow Sea but are exacerbated by domestic pollution produced near SMA. This emphasizes a reevaluation of domestic emission controls, in particular reactive aromatics such as toluene (e.g., toluene not only contributes to the $P(O_3)$ shown herein, but also contributes to 9 % of modeled secondary organic aerosol over SMA; Nault et al., 2018). Organic aerosol formation has also been recently investigated during the KORUS-AQ study period to estimate relationships between in situ observations and satellite derived products (e.g., formaldehyde; Liao et al., 2019). These findings are in line with the detailed Rapid Science Synthesis Report (https://kr.usembassy.gov/wp-content/uploads/sites/75/2017/07/KORUS-AQ-RSSR.pdf, last access: 27 March 2019) that provides findings from the KORUS-AQ study which are intended to be useful for policy makers as they develop air quality mitigation strategies and continue to identify specific emission sources that should be targeted for reduction. Direct observations of free tropospheric O_3 were rarely observed below 60 ppbv during the KORUS-AQ study period (see Figs. 4c and 12), indicating that the baseline conditions on which South Korean national regulatory standards are predicated are trending (Cooper et al., 2014) towards a regime where they are increasingly unattainable. In order to further assess transboundary pollution, emission sources, and plume evolution, there has been an international effort to launch the Geostationary Environmental Monitoring Spectrometer (GEMS) to provide hourly measurements of key pollutants (e.g., O_3, NO_2, SO_2, and particulate matter) over the Korean

peninsula and the Asia–Pacific region. The KORUS-AQ analyses offer an exemplary synergistic approach on how to collect the statistics required by the regulatory agencies of Korea to improve air quality in both urban and rural settings.

Author contributions. JTS, TJM, RMS, AMT, LT, and GS designed and executed field measurements for collecting surface O_3, O_3 lidar, and ozonesondes at TRF. AnW provided the airborne O_3 and NO_2 data. ArW provided the airborne PTR-To-MS data. CK ran the FLEXPART analysis. SJ provided the GeoTASO data. RL, JS, and TK provided surface and ceilometer data. SK, DJ, and DS provided the PTR-ToF-MS data and logistical support. JRS provide the photochemical modeling analysis. JP and YL provided additional surface measurements at TRF and OLY. JTS prepared the original manuscript, and all other authors contributed in editing the paper.

References

Brioude, J., Arnold, D., Stohl, A., Cassiani, M., Morton, D., Seibert, P., Angevine, W., Evan, S., Dingwell, A., Fast, J. D., Easter, R. C., Pisso, I., Burkhart, J., and Wotawa, G.: The Lagrangian particle dispersion model FLEXPART-WRF version 3.1, Geosci. Model Dev., 6, 1889–1904, https://doi.org/10.5194/gmd-6-1889-2013, 2013.

Choi, K.-C., Lee, J.-J., Bae, C. H., Kim, C.-H., Kim, S., Chang, L.-S., Ban, S.-J., Lee, S.-J., Kim, J., and Woo, J.-H.: Assessment of transboundary ozone contribution toward South Korea using multiple source–receptor modeling techniques, Atmos. Environ., 92, 118–129, 2014.

Cooper, O. R., Parrish, D. D., Ziemke, J., Balashov, N. V., Cupeiro, M., Galbally, I. E., Gilge, S., Horowitz, L., Jensen, N. R., Lamarque, J.-F., Naik, V., Oltmans, S. J., Schwab, J., Shindell, D. T., Thompson, A. M., Thouret, V., Wang, Y., and Zbinden, R. M.: Global distribution and trends of tropospheric ozone: An observation-based review. Elem Sci Anth, 2, 000029, https://doi.org/10.12952/journal.elementa.000029, 2014.

Duncan, B. N., Lamsal, L. N., Thompson, A. M., Yoshida, Y., Lu, Z., Streets, D. G., Hurwitz, M. M., and Pickering, K. E.: A spacebased, high-resolution view of notable changes in urban NO_x pollution around the world (2005–2014), J. Geophys. Res.-Atmos., 121, 976–996, 2016.

Gelaro, R., McCarty, W., Suárez, M. J., Todling, R., Molod, A., Takacs, L., Randles, C. A., Darmenov, A., Bosilovich, M. G., Reichle, R., Wargana, K., Coy., L., Cullather, R., Draper, C., Akella, S., Buchard, V., Conaty, A., da Silva, A. M., Gu, W., Kim, G.-K., Koster, R., Lucchesi, R., Merkova, D., Nielsen, J. E., Partyka, G., Pawson, S., Putman, W., Rienecker, M., Schubert, S. D., Sienkiewicz, M., and Zhao, B.: The modern-era retrospective analysis for research and applications, version 2 (MERRA-2), J. Climate, 30, 5419–5454, 2017.

Ghim, Y. S. and Chang, Y. S.: Characteristics of ground-level ozone distributions in Korea for the period of 1990–1995, J. Geophys. Res.-Atmos., 105, 8877–8890, 2000.

Ghim, Y. S., Moon, K. C., Lee, S., and Kim, Y. P.: Visibility trends in Korea during the past two decades, J. Air Waste Manage. Assoc., 55, 73–78, 2005.

He, H., Li, C., Loughner, C. P., Li, Z., Krotkov, N. A., Yang, K., Wang, L., Zheng, Y., Bao, X., Zhao, G., and Dickerson, R. R.: SO_2 over central China: Measurements, numerical simulations and the tropospheric sulfur budget, J. Geophys. Res.-Atmos., 117, D16, https://doi.org/10.1029/2011JD016473, 2012.

Herman, J., Spinei, E., Fried, A., Kim, J., Kim, J., Kim, W., Cede, A., Abuhassan, N., and Segal-Rozenhaimer, M.: NO_2 and HCHO measurements in Korea from 2012 to 2016 from Pandora spectrometer instruments compared with OMI retrievals and with aircraft measurements during the KORUS-AQ campaign, Atmos. Meas. Tech., 11, 4583–4603, https://doi.org/10.5194/amt-11-4583-2018, 2018.

Huang, M., Crawford, J. H., Diskin, G. S., Santanello, J. A., Kumar, S. V., Pusede, S. E., Parrington, M., and Carmichael, G. R.: Modeling Regional Pollution Transport Events During KORUS-AQ: Progress and Challenges in Improving Representation of Land-Atmosphere Feedbacks, J. Geophys. Res.-Atmos., 123, 10–732, 2018.

Iqbal, M. A., Kim, K.-H., Shon, Z.-H., Sohn, J.-R., Jeon, E.-C., Kim, Y.-S., and Oh, J.-M.: Comparison of ozone pollution levels

at various sites in Seoul, a megacity in Northeast Asia, Atmos. Res., 138, 330–345, 2014.

Jeon, W. B., Lee, S. H., Lee, H. W., and Kim, H. G.: Process analysis of the impact of atmospheric recirculation on consecutive high-O_3 episodes over the Seoul Metropolitan Area in the Korean Peninsula, Atmos. Environ., 63, 213–222, 2012.

Jeon, W.-B., Lee, S.-H., Lee, H., Park, C., Kim, D.-H., and Park, S.-Y.: A study on high ozone formation mechanism associated with change of NO_x/VOCs ratio at a rural area in the Korean Peninsula, Atmos. Environ., 89, 10–21, 2014.

Jeong, D., Seco, R., Gu, D., Lee, Y., Nault, B. A., Knote, C. J., Mcgee, T., Sullivan, J. T., Jimenez, J. L., Campuzano-Jost, P., Blake, D. R., Sanchez, D., Guenther, A. B., Tanner, D., Huey, L. G., Long, R., Anderson, B. E., Hall, S. R., Ullmann, K., Shin, H.-J., Herndon, S. C., Lee, Y., Kim, D., Ahn, J., and Kim, S.: Integration of Airborne and Ground Observations of Nitryl Chloride in the Seoul Metropolitan Area and the Implications on Regional Oxidation Capacity During KORUS-AQ 2016, Atmos. Chem. Phys. Discuss., https://doi.org/10.5194/acp-2018-1216, in review, 2018.

Kim, H., Zhang, Q., and Heo, J.: Influence of intense secondary aerosol formation and long-range transport on aerosol chemistry and properties in the Seoul Metropolitan Area during spring time: results from KORUS-AQ, Atmos. Chem. Phys., 18, 7149–7168, https://doi.org/10.5194/acp-18-7149-2018, 2018.

Kim, S.: Fast Oxidation of reactive gases in the lower troposphere above a forest downwind of an Asian megacity, Environ. Sci. Technol., in review, 2018.

Kim, S., Karl, T., Guenther, A., Tyndall, G., Orlando, J., Harley, P., Rasmussen, R., and Apel, E.: Emissions and ambient distributions of Biogenic Volatile Organic Compounds (BVOC) in a ponderosa pine ecosystem: interpretation of PTR-MS mass spectra, Atmos. Chem. Phys., 10, 1759–1771, https://doi.org/10.5194/acp-10-1759-2010, 2010.

Kim, S., Kim, S.-Y., Lee, M., Shim, H., Wolfe, G. M., Guenther, A. B., He, A., Hong, Y., and Han, J.: Impact of isoprene and HONO chemistry on ozone and OVOC formation in a semirural South Korean forest, Atmos. Chem. Phys., 15, 4357–4371, https://doi.org/10.5194/acp-15-4357-2015, 2015.

Kim, S.-W., Yoon, S.-C., Won, J.-G., and Choi, S.-C.: Ground-based remote sensing measurements of aerosol and ozone in an urban area: A case study of mixing height evolution and its effect on ground-level ozone concentrations, Atmos. Environ., 41, 7069–7081, 2007.

Kim, S. Y., Lee, J. T., Hong, Y. C., Ahn, K. J., and Kim, H.: Determining the threshold effect of ozone on daily mortality: an analysis of ozone and mortality in Seoul, Korea, 1995–1999, Environ. Res., 94, 113–119, 2004.

Kim, S.-Y., Seo, S.-J., Park, H.-J., Son, J.-S., Park, J.-H., and Kim, J.-C.: Airborne measurements of ozone and its precursors over Yeosu- Gwangyang industrial areas in the Southern Coast of Korea, Asian J. Atmos. Environ., 7, 139–151, 2013.

Kuang, S., Newchurch, M. J., Thompson, A. M., Stauffer, R. M., Johnson, B. J., and Wang, L.: Ozone variability and anomalies observed during SENEX and SEAC4RS campaigns in 2013, J. Geophys. Res.-Atmos., 122, 227–241, 2017.

Lee, C., Richter, A., Lee, H., Kim, Y. J., Burrows, J. P., Lee, Y. G., and Choi, B. C.: Impact of transport of sulfur dioxide from the Asian continent on the air quality over Korea during May 2005, Atmos. Environ., 42, 1461–1475, 2008.

Lee, D.-G., Lee, Y.-M., Jang, K.-W., Yoo, C., Kang, K.-H., Lee, J.-H., Jung, S.-W., Park, J.-M., Lee, S.-B., Han, J.-S., Hong, J.-H., and Lee, S.-J: Korean national emissions inventory system and 2007 air pollutant emissions, Asian J. Atmos. Environ., 5, 278–291, 2011.

Lee, J.-T., Kim, H., Hong, Y.-C., Kwon, H.-J., Schwartz, J., and Christiani, D. C.: Air pollution and daily mortality in seven major cities of Korea, 1991–1997, Environ. Res., 84, 247–254, 2000.

Lee, K.-Y., Kwak, K.-H., Ryu, Y.-H., Lee, S.-H., and Baik, J.-J.: Impacts of biogenic isoprene emission on ozone air quality in the Seoul metropolitan area, Atmos. Environ., 96, 209–219, 2014.

Lennartson, E. M., Wang, J., Gu, J., Castro Garcia, L., Ge, C., Gao, M., Choi, M., Saide, P. E., Carmichael, G. R., Kim, J., and Janz, S. J.: Diurnal variation of aerosol optical depth and $PM_{2.5}$ in South Korea: a synthesis from AERONET, satellite (GOCI), KORUS-AQ observation, and the WRF-Chem model, Atmos. Chem. Phys., 18, 15125–15144, https://doi.org/10.5194/acp-18-15125-2018, 2018.

Liao, J., Hanisco, T. F., Wolfe, G. M., St. Clair, J., Jimenez, J. L., Campuzano-Jost, P., Nault, B. A., Fried, A., Marais, E. A., Gonzalez Abad, G., Chance, K., Jethva, H. T., Ryerson, T. B., Warneke, C., and Wisthaler, A.: Towards a satellite formaldehyde – in situ hybrid estimate for organic aerosol abundance, Atmos. Chem. Phys., 19, 2765–2785, https://doi.org/10.5194/acp-19-2765-2019, 2019.

Lim, Y.-J., Armendariz, A., Son, Y.-S., and Kim, J.-C.: Seasonal variations of isoprene emissions from five oak tree species in East Asia, Atmos. Environ., 45, 2202–2210, 2011.

Miyazaki, K., Eskes, H. J., Sudo, K., Takigawa, M., van Weele, M., and Boersma, K. F.: Simultaneous assimilation of satellite NO_2, O_3, CO, and HNO_3 data for the analysis of tropospheric chemical composition and emissions, Atmos. Chem. Phys., 12, 9545–9579, https://doi.org/10.5194/acp-12-9545-2012, 2012.

Miyazaki, K., Sekiya, T., Fu, D., Bowman, K., Kulawik, S., Sudo, K., Walker, T., Kanaya, Y., Takigawa, M., Ogochi, K., Eskes, H., Boersma, K. F., Thompson, A. M., Gaubert, B., Barre, J., and Emmons, L. K.: Balance of emission and dynamical controls on ozone during KORUS-AQ from multi-constituent satellite data assimilation, J. Geophys. Res.-Atmos., 124, 387–413, 2018.

Müller, M., Mikoviny, T., Feil, S., Haidacher, S., Hanel, G., Hartungen, E., Jordan, A., Märk, L., Mutschlechner, P., Schottkowsky, R., Sulzer, P., Crawford, J. H., and Wisthaler, A.: A compact PTR-ToF-MS instrument for airborne measurements of volatile organic compounds at high spatiotemporal resolution, Atmos. Meas. Tech., 7, 3763–3772, https://doi.org/10.5194/amt-7-3763-2014, 2014.

Nault, B. A., Campuzano-Jost, P., Day, D. A., Schroder, J. C., Anderson, B., Beyersdorf, A. J., Blake, D. R., Brune, W. H., Choi, Y., Corr, C. A., de Gouw, J. A., Dibb, J., DiGangi, J. P., Diskin, G. S., Fried, A., Huey, L. G., Kim, M. J., Knote, C. J., Lamb, K. D., Lee, T., Park, T., Pusede, S. E., Scheuer, E., Thornhill, K. L., Woo, J.-H., and Jimenez, J. L.: Secondary organic aerosol production from local emissions dominates the organic aerosol budget over Seoul, South Korea, during KORUS-AQ, Atmos. Chem. Phys., 18, 17769–17800, https://doi.org/10.5194/acp-18-17769-2018, 2018.

Nowlan, C. R., Liu, X., Leitch, J. W., Chance, K., González Abad, G., Liu, C., Zoogman, P., Cole, J., Delker, T., Good, W., Murcray, F., Ruppert, L., Soo, D., Follette-Cook, M. B., Janz, S. J., Kowalewski, M. G., Loughner, C. P., Pickering, K. E., Herman, J. R., Beaver, M. R., Long, R. W., Szykman, J. J., Judd, L. M., Kelley, P., Luke, W. T., Ren, X., and Al-Saadi, J. A.: Nitrogen dioxide observations from the Geostationary Trace gas and Aerosol Sensor Optimization (GeoTASO) airborne instrument: Retrieval algorithm and measurements during DISCOVER-AQ Texas 2013, Atmos. Meas. Tech., 9, 2647–2668, https://doi.org/10.5194/amt-9-2647-2016, 2016.

Ryu, Y.-H., Baik, J.-J., Kwak, K.-H., Kim, S., and Moon, N.: Impacts of urban land-surface forcing on ozone air quality in the Seoul metropolitan area, Atmos. Chem. Phys., 13, 2177–2194, https://doi.org/10.5194/acp-13-2177-2013, 2013.

Schroeder, J. R., Crawford, J. H., Fried, A., Walega, J., Weinheimer, A., Wisthaler, A., Müller, M., Mikoviny, T., Chen, G., Shook, M., Blake, D. R., Diskin, G., Estes, M., Thompson, A. M. Lefer, B., L., Long, R., and Mattson, E.: Formaldehyde column density measurements as a suitable pathway to estimate near-surface ozone tendencies from space, J. Geophys. Res.-Atmos., 121, 13088–13112, 2016.

Seo, J., Youn, D., Kim, J. Y., and Lee, H.: Extensive spatiotemporal analyses of surface ozone and related meteorological variables in South Korea for the period 1999–2010, Atmos. Chem. Phys., 14, 6395–6415, https://doi.org/10.5194/acp-14-6395-2014, 2014.

Stauffer, R. M., Thompson, A. M., and Young, G. S.: Tropospheric ozonesonde profiles at long-term US monitoring sites: 1. A climatology based on self-organizing maps, J. Geophys. Res.-Atmos., 121, 1320–1339, 2016.

Sullivan, J. T., McGee, T. J., Sumnicht, G. K., Twigg, L. W., and Hoff, R. M.: A mobile differential absorption lidar to measure sub-hourly fluctuation of tropospheric ozone profiles in the Baltimore-Washington, D.C. region, Atmos. Meas. Tech., 7, 3529–3548, https://doi.org/10.5194/amt-7-3529-2014, 2014.

Sullivan, J. T., McGee, T. J., De Young, R., Sumnicht, G. K., Twigg, L. W., Pliutau, D., Carrion, W., and Knepp, T.: Results from the NASA GSFC and LaRC ozone lidar intercomparison: New mobile tools for atmospheric research, J. Atmos. Ocean. Tech., 32, 1779–1795, 2015a.

Sullivan, J. T., McGee, T. J., Leblanc, T., Sumnicht, G. K., and Twigg, L. W.: Optimization of the GSFC TROPOZ DIAL retrieval using synthetic lidar returns and ozonesondes – Part 1: Algorithm validation, Atmos. Meas. Tech., 8, 4133–4143, https://doi.org/10.5194/amt-8-4133-2015, 2015b.

Sullivan, J. T., McGee, T. J., Thompson, A. M., Pierce, R. B., Sumnicht, G. K., Twigg, L. W., Eloranta, E., and Hoff, R. M.: Characterizing the lifetime and occurrence of stratospheric-tropospheric exchange events in the rocky mountain region using high-resolution ozone measurements, J. Geophys. Res.-Atmos., 120, 12410–12424, 2015c.

Sullivan, J. T., McGee, T. J., Langford, A. O., Alvarez, R. J., Senff, C. J., Reddy, P. J., Thompson, A. M., Twigg, L. W., Sumnicht, G. K., Lee, P., Weinheimer, A., Knote, C., Long, R. W., and Hoff, R. M.: Quantifying the contribution of thermally driven recirculation to a high-ozone event along the Colorado Front Range using lidar, J. Geophys. Res.-Atmos., 121, 10–377, 2016.

Sullivan, J. T., Rabenhorst, S. D., Dreessen, J., McGee, T. J., Delgado, R., Twigg, L., and Sumnicht, G.: Lidar observations revealing transport of O$_3$ in the presence of a nocturnal low-level jet: Regional implications for "next-day" pollution, Atmos. Environ., 158, 160–171, 2017.

Thompson, A. M., Witte, J. C., Smit, H. G., Oltmans, S. J., Johnson, B. J., Kirchhoff, V. W., and Schmidlin, F. J.: Southern Hemisphere Additional Ozonesondes (SHADOZ) 1998–2004 tropical ozone climatology: 3. Instrumentation, station-to-station variability, and evaluation with simulated flight profiles, J. Geophys. Res.-Atmos., 112, D3, 2007.

Thompson, A. M., Smit, H. G., Witte, J. C., Stauffer, R. M., Johnson, B. J., Morris, G., von der Gathen, P., Van Malderen, R., Davies, J., Piters, A., Allaart, M., Posny, F., Kivi, R., Cullis, P., Hoang Anh, N. T., Corrales, E., Machinini, T., da Silva, F. R., Paiman, G., Thiongó, K., Zainal, Z., Brothers, G. B., Wolff, K. R., Nakano, T., Stübi, R., Romanens, G., Coetzee, G. J., Diaz, J. A., Mitro, S., Mohamad, M., and Ogino, S.: Ozonesonde Quality Assurance: The JOSIE-SHADOZ (2017) Experience, Bull. Amer. Meteor. Soc., 100, 155–171, https://doi.org/10.1175/BAMS-D-17-0311.1, 2019.

Vellingiri, K., Kim, K.-H., Jeon, J. Y., Brown, R. J., and Jung, M.-C.: Changes in NO$_x$ and O$_3$ concentrations over a decade at a central urban area of Seoul, Korea, Atmos. Environ., 112, 116–125, 2015.

Wang, S. X., Zhao, B., Cai, S. Y., Klimont, Z., Nielsen, C. P., Morikawa, T., Woo, J. H., Kim, Y., Fu, X., Xu, J. Y., Hao, J. M., and He, K. B.: Emission trends and mitigation options for air pollutants in East Asia, Atmos. Chem. Phys., 14, 6571–6603, https://doi.org/10.5194/acp-14-6571-2014, 2014.

Wang, X. and Mauzerall, D. L.: Characterizing distributions of surface ozone and its impact on grain production in China, Japan and South Korea: 1990 and 2020, Atmos. Environ., 38, 4383–4402, 2004.

Weinheimer, A. J.: Chemical methods: chemiluminescence, chemical amplification, electrochemistry, and derivatization, Analytical Techniques for Atmospheric Measurement, 311 pp., 2006.

Witte, J. C., Thompson, A. M., Smit, H. G., Fujiwara, M., Posny, F., Coetzee, G. J., Northam, E. T., Johnson, B. J., Sterling, C. W., Mohamad, M., and Ogino, S. Y.: First reprocessing of Southern Hemisphere ADditional OZonesondes (SHADOZ) profile records (1998–2015): 1. Methodology and evaluation, J. Geophys. Res.-Atmos., 122, 6611–6636, 2017.

Zhao, Y., Wang, S., Duan, L., Lei, Y., Cao, P., and Hao, J.: Primary air pollutant emissions of coal-fired power plants in China: Current status and future prediction, Atmos. Environ., 42, 8442–8452, 2008.